Expansion of the Hadley cell under global warming

Jian Lu[1] Gabriel A. Vecchi[2] Thomas Reichler[3]

[1]UCAR Postdoctoral Fellow/Visiting Scientist at GFDL/NOAA
P.O. Box 308, Princeton University, Princeton, NJ 08542

[2]Geophysical Fluid Dynamical Laboratory, National Oceanic and Atmospheric Administration, P.O. Box 308, Princeton University, Princeton, NJ 08542

[3]Department of Meteorology, University of Utah, 135 S 1460E, Room 819 (WBB), Salt Lake City, UT 84112-0110

Corresponding author:
Dr. Jian Lu
UCAR Visiting Scientist
GFDL/NOAA
Princeton University Forrestal Campus, US Route 1
P.O. Box 308
Princeton, NJ 08542
Email: Jian.Lu@noaa.gov

Abstract

Consistent weakening and poleward expansion of the Hadley circulation are diagnosed in climate change simulations of the IPCC AR4 project. Associated with this widening is a concomitant poleward expansion of the subtropical dry zone. Simple scaling analysis supports the notion that the poleward extent of the Hadley cell is set by the location where the thermally driven jet first becomes baroclinically unstable. The expansion of the Hadley cell is caused by an increase in the subtropical static stability, which pushes poleward the baroclinic instability zone and hence the outer boundary of the Hadley cell.

1. Introduction

The Hadley cell (HC) plays a pivotal role in the earth's climate by transporting energy and angular momentum poleward and by organizing the three dimensional tropical atmospheric circulation. The locations of the large-scale subtropical dry zones and the major tropical/subtropical deserts of the globe are largely determined by the subsiding branches of the HC. Thus, understanding how the structure and intensity of the HC and the associated subtropical dry zones may change under the greenhouse gas (GHG)-induced global warming is a topic of substantial interest.

The detailed response of the HC to increasing GHG is complex, as the HC is influenced by many factors, involving tropical heating processes [e.g., Mitas and Clement, 2006], the atmospheric stability [e.g., Schneider, 1977], extra-tropical eddy dynamics [e.g., Walker and Schneider, 2006], and total atmospheric moisture [Frierson et al., 2006]. To date, studies of the long term behavior of the HC, and the extent to which GHG forcing is relevant remain inconclusive. Atmospheric reanalyses show a statistically significant intensification of their Hadley circulation throughout the second part of the 20th century [Mitas and Clement, 2005]. However, this intensification is not found in the rawinsonde data, nor in most 20th century simulations using both coupled or atmosphere-only general circulation models (GCMs) [Mitas and Clement, 2005; 2006]. Meanwhile, simple physical arguments (e.g., Betts, 1998; Knutson and Manabe, 1995; Held and Soden [2006] predict slowdown of the overall tropical overturning circulation under global warming. Such a slowdown seems to be a robust feature in GCMs [Vecchi and Soden, 2006] and has been identified in observational analyses of the Walker circulation [Vecchi et al., 2006; Zhang and Song, 2006]. However, it remains to be seen whether it also projects onto the zonally averaged part of the circulation. As far as the structure of the HC is concerned, analysis of the satellite observations indicates that the HC has been expanding poleward over the past 27 years [Fu et al. 2006]. Whether this observation is an integral part of the response to GHG warming is not clear and warrants further investigation.

Here, we investigate the response of the HC to global warming using 21st century increasing GHG scenarios from the Fourth Assessment Report (AR4) of the Intergovernmental Panel on Climate Change (IPCC). The various AR4 models and the associated diversity in their numerical schemes, parameterizations, and other physics provide a unique opportunity for this task. In this study we will show that there is a robust poleward expansion and weakening of the Hadley circulation across all models and we will identify possible mechanisms for this behavior.

2. Data and Methods

Gridded global monthly precipitation, evaporation, surface air temperature, surface wind, temperature, and 500hPa pressure velocity (ω_{500}) are retrieved from the AR4 archive website (http://www-pcmdi.llnl.gov), and annual means are formed for the analysis. Most of our analysis is based on output from the A2 scenario which is at the upper end of GHG emission (the CO_2 concentration reaches 800 ppm at the end of the 21st century). Only the first ensemble member of each of the 14-15 models (depending on the availability of the variables) is used. To identify the climate change response, we compare the first and last twenty years of the 21st century, i.e., (2081-2100) minus (2001-2020).

To determine the poleward edges of the HC, we compute the zonal-mean mass flux stream function (ψ) by vertically integrating the density-weighted meridional wind component from the top model level downward. We first determine the maximum absolute value of this streamfunction at 500 hPa (ψ_{500}), and then identify the edges of the HC as the first latitude poleward of the maximum at which ψ_{500} becomes zero. An alternative definition of the HC edge as the transition latitude from zonal-mean surface easterlies to westerlies is also tested and does not influence the principal conclusions of this study. Therefore, only the results from the ψ_{500} based definition are presented here. The intensity of Hadley Cell (IHC) is measured from the meridional integral of the upward branch of the zonally integrated 500hPa omega field in the tropics, i.e., $\int\left(\int \omega_{500} dx\right)^{+} dy$ or equivalently, the difference between the maximum and minimum of ψ_{500}, i.e., $\psi_{500}^{\max} - \psi_{500}^{\min}$. Finally, the edge of the subtropical dry zone in each hemisphere is identified as the latitude where the zonal mean precipitation minus evaporation (*P-E*) field crosses zero when increasing from the subtropical minimum poleward.

Theories of the Hadley circulation suggest that the meridional extent of the HC should scale with the height of the tropopause [Held and Hou, 1980, Held, 2000]. This height is computed from temperature data as the lowest pressure level at which the lapse rate decreases to 2°C/km, following the algorithm of Reichler et al. [2003] and the WMO (1957) definition.

To account for the different climate sensitivities of each model, we normalize, at times, the various quantities by the corresponding changes in global mean surface temperature of each model.

3. Results

We first examine the response of global hydrological cycle in scenario A2 by looking at the field of precipitation minus evaporation (P-E). As shown by Fig.1, the overall characteristic of the multi-model ensemble mean hydrological response to global warming is a reinforcement of the global climatological background pattern (Held and Soden, 2006). For clarity, areas of negative climatological *P-E* are hatched. In addition, there is a general tendency for a poleward expansion of the subtropical dry zone (areas encircled by the 0 isopleths of *P-E*). Counting the number of models that simulate a positive P-E change (Fig.1b), one can see that the overall pattern of *P-E* change is robust across most models and that the model number count bears great resemblance to the trend pattern itself.

The poleward expansion of the subtropical dry zone is strongly tied to the poleward expansion of the HC (see Fig.2). Based on the 38 simulations from the three scenarios (A2, A1B, B1), about 85% (72%) of the spread in the poleward displacement of the subtropical dry zones in the southern (northern) hemisphere can be explained by a linear relation to the displacements of the outer boundaries of the HC. The ensemble mean response of the A2 scenario (open circle) shows that the edges of the subtropical dry zone displace poleward by ~1° in each hemisphere. A similar poleward expansion can be found in the subtropical downward ω_{500} field (not shown). The magnitude of the expansion is a function of the GHG forcing, with similar but weaker expansions found in scenarios A1B (hexagrams) and B1 (triangles), which correspond to the CO2 stabilization at 720 ppm and 550 ppm, respectively.

Another important aspect of the HC response to global warming is the reduction of its intensity (Fig.3). The models show a tendency for a HC weakening at rates between 0-4%/K, with a mean of 1.2%/K. It is important to note that these models predict a slowdown of the entire tropical overturning circulation, particularly the Walker circulation [Vecchi and Soden, 2006], in a manner consistent with the discussion in Held and Soden (2006). Meanwhile, weakening of the HC (~1%/K) is substantially smaller than that of the Walker circulation (~5%/K, Vecchi and Soden, 2006) for reasons yet to be understood. Interestingly, a similar anisotropism is also found in the reduction of the zonal mean and the zonally asymmetric components of the tropical convective mass flux (Held and Soden, 2006).

4. Possible mechanisms for HC expansion

Much of the understanding of the HC has been built on two alternative views on the controls of the width of the HC. On one hand, nearly inviscid theory for axisymmetric circulation (no eddies) [Held and Hou 1980] predicts that the meridional extent of the HC scales as

$$\phi_H \sim \left(\frac{gH_t}{\Omega^2 a^2} \frac{\Delta_h}{\theta_0} \right)^{\frac{1}{2}}, \qquad (1)$$

where H_t is the height of the tropical tropopause, θ_0 is global mean temperature, Δ_h is the equator-to-pole surface potential temperature difference in radiative equilibrium, and other parameters have their conventional meanings. This scaling relation, which suggests no dependence on static stability, is derived by assuming that (i) the zonal wind in the upper branch of the HC is angular-momentum conserving and (ii) the HC is energetically closed, so that the diabatic heating in the ascent regions is balanced by the diabatic cooling in the descent regions. The second view sees the width of the HC as being determined by the poleward extent to which the angular-momentum conservation continues until the resulting vertical shear becomes baroclinically unstable [Held, 2000]. Solving the equation between the angular momentum conserving zonal wind and the baroclinically critical zonal wind yields an alternative scaling for the width of the HC:

$$\phi_H \propto \left(\frac{NH_e}{\Omega a} \right)^{\frac{1}{2}}, \qquad (2a)$$

if using the two-layer model's criterion (Phillips, 1954) for instability, or

$$\phi_H \propto \left(\frac{NH_e}{\Omega^2 a} \right)^{\frac{1}{3}}, \qquad (2b)$$

if using a more general criterion based on the Eady growth rate[1], both implying a positive proportional relationship with NH_e. Here, H_e is the local tropopause height where the instability first occurs; N is the vertically averaged Brunt-Väisälä frequency, indicative of the tropospheric gross static stability. If the scaling relation (1) applies to the HC expansion under GHG forcing, variations of the HC width should be proportional to the tropical tropopause height[2]. On the other hand, if the scaling (2) applies, one may expect the extent of the Hadley circulation to be sensitive to the gross stability and the tropopause height near the poleward boundary of the circulation.

First, to test the extent to which scaling relation (1) controls the models' HC expansion through changing the tropical tropopause height (TTH), we plot for each model the change in TTH during the 21st century against that of the HC extent, the former being estimated as the negative of the pressure anomalies at the tropopause and averaged within 20° to the equator, and the latter defined as the distance between the southern and northern edges of the HC. Both quantities have been normalized by the increase of the global mean temperature seen in the individual models during the 21st century. Comparing different models, the individual long-term trends in HC extent show only a small correlation to the trends in TTH (Fig.4a). In fact, within each model, the detrended annual mean time series of TTH and HC extent tend to be anti-correlated, in stark contrast to the positive correlations of the time series with trend (Fig.4b). This hints at

[1] Eady growth rate used here is a version in vertical average sense, i.e., fu / NH , where u is the zonal wind difference between the upper and lower troposphere.

[2] From scaling relation (1), neither the increased global mean temperature θ_0, nor the extratropical amplification of the global warming signal, which decreases Δ_h, are likely to have direct contribution to the widening of the Hadley cell.

distinct mechanisms between that governs the long-term widening of the HC under global warming and that governs its interannual variability. Further composite analysis using the simulations from GFDL CM2.1 model (not shown) reveals that, at interannual time scales, anomalously high TTH is associated with El Niño-like conditions — stronger and narrower than normal tropical heating and more intensive Hadley overturning circulation. This is consistent with previous findings [Chang, 1995; Seager et al. 2002] that the more accentuated tropical convective heating during El Niño usually drives a stronger and narrower HC.

On the other hand, the extratropical tropopause height (ETH, averaged over 35°-55°), is found to be closely related to the variation of the HC extent not only within each model (Fig.4d), but also in the comparison of the long-term trend among models (Fig.4c). A similar relationship has been found between the HC extent and the gross stability. Indeed, the ETH is very strongly correlated with the local gross stability (with correlations of ~0.95) within most models examined and hence can be thought of as a good proxy of the ETH. The change in mid-latitude tropopause height (or stability) not only explains over 60% of the variance in the spread of the HC widening across the AR4 models, but also accounts for the consensus HC expansion at a rate of 1.2° per 10hPa rise in the ETH in the A2 scenario. The relevance of the ETH to the HC extent in the natural climate variability can also be readily discerned from their correlations of the detrended time series in Fig.4d.

From this analysis, one is attempted to argue that scaling relation (2) is a better model for the extent of the HC. The HC in the present-day climate may better be interpreted as being limited by where the thermally driven wind becomes baroclinically unstable than by the energetic closure of the thermally driven cell.

5. Concluding Remarks

In response to increased GHG forcing, we find a robust weakening and poleward expansion of the Hadley circulation in simulations of the 21^{st} century climate taken from the A2 scenario of the IPCC AR4 project. In accord with the movement of the HC, the subtropical dry zones also expand poleward. Further analysis suggests that the consensus of the HC expansion in the AR4 models is unlikely to originate from tropical processes, despite the fact that tropical heating is effective in driving the variation of the HC at ENSO time scales, and that it accounts for significant part of the spread in the expansion rate among models (not shown). We find that extratropical tropopause height, as a good proxy of the gross static stability, varies in concert with the width of the HC on both the interannual and longer time scales. The increase in the gross stability near the subtropics decreases the baroclinic instability, a critical factor that controls the limits the outer boundaries of the HC. This postpones the thermally driven cell to break down at high latitude, and as a result, the edges of the HC expand poleward.

The latitudinal distribution of the lower tropospheric warming in the A2 scenario runs shows remarkable qualitative resemblance to observational estimates from the microwave sounding unit (MSU) data gathered over the period 1979-2005 [Fu et al., 2006], both sharing features such as a local minimum warming near the equator, a local maximum warming in the subtropics, and amplified warming in the Northern Hemisphere high-latitudes. The details of the warming profile are important, because they are associated with poleward shift of the subtropical jets and poleward expansion of the HC, the exact phenomena diagnosed in this study from the global warming simulations. Fu et al. [2006] estimated the amount of latitudinal widening of the HC over the period 1979-2005 as ~2° latitude. Over the same period the increase in global temperature was about 0.5°C, so that the widening of the HC amounts to ~4° latitude per degree warming. This is much greater than what we find in the simulations of the AR4 A2 scenario (~0.6° latitude /K). Thus, the observed expansion of the Hadley circulation during the late 20th century may, to a large degree, be attributed to factors other than the GHG-induced global warming, such as ozone depletion and/or natural climate variability. It is also possible that the contribution from the GHG forcing may be larger than the ensemble mean suggests, given the large spread between the individual model simulations (Fig.4).

Interestingly, the model-based projection of a expanding HC is also consistent with the paleoclimate record. It has been argued that the boundaries of the HC were further poleward during the warm Cretaceous climate [Farrell, 1990], and further equatorward during glacial periods [Chylek et al. 2001; Williams and Bryan, 2006].

Acknowledgement

We thank Kirk Bryan, Isaac Held, Dargan Frierson, and Qian Song for their perceptive comments and useful discussions during the formative stage of this paper. We acknowledge the international modeling group for providing their data for analysis, the Program for Climate Model Diagnosis and Intercomparison (PCMDI) for collecting and archiving the model data, the JSC/CLIVAR Working Group on Coupled Modeling (WGCM) and their Coupled Model Intercomparison Project (CMIP) and Climate Simulation Panel for organizing the model data and analysis activity, and the IPCC WG1 TSU for technical support. The IPCC Data Archive at Lawrence Livermore National Laboratory is supported by the Office of Science, U. S. Department of Energy. J. Lu is supported by the Visiting Scientist Program of the University Corporation for Atmospheric Research (UCAR). T. Reichler is partially supported by NSF grant ATM 0532280.

References

Betts, A. K., 1998, Climate-convection feedbacks: some further issues, Climatic Change, **39**, 35-38

Chang, E. K. M., 1995, The influence of Hadley circulation intensity changes on extratropical climate in an idealized model. *J. Atmos. Sci.*, **52,** 2006-2024

Chylek, P., G. Lesins, and U. Lohmann, 2001, Ehancement of dust source area during past glacial periods due to changes of the Hadley circulation. *J. Geophys. Res.*, **106** (D16), 18447-18485

Farrell, B. F., 1990, Equable climate dynamics, *J. Atmos. Sci.*, **47,** 2986-2995

Frierson, D. M. W., I. Held, P. Zurita-Gotor, 2006, A gray-radiation aquaplanet moist GCM. Part I: Static stability and eddy scale, *J. Atmos. Sci.*, (submitted)

Fu, Q., C. M. Johanson, J. M. Wallace, and T. Reichler, 2006, Enhanced mid-latitude tropospheric warming in satellite measurements. *Science,* **312**, 1179

Held, I. M., 2000, The general circulation of the atmosphere. *Proc. Program in Geophysical Fluid Dynamics.* Woods Hole Oceanographic Institution, Wood Hole, MA. http://gfd.whoi.edu/proceedings/2000/PDFvol2000.html

Held, I. M. and A. Y. Hou, 1980, Nonlinear axially symmetric circulations in a nearly inviscid atmosphere, *J. Atmos. Res.,* **37,** 515-533

Held, I. M. and B. J. Soden, 2006, Robust response of the hydrological cycle to global warming, *J. Clim.,* (in press)

Knutson, T. R. and S. Manabe, 1995, Time-mean response over the tropical Pacific to increased CO2 in a coupled ocean-atmosphere model, *J. Clim.*, **8**, 2181-2199

Mitas, C. M. and A. Clement, 2005, Has the Hadley cell been strengthening in recent decades? *Goephys. Res. Lett.,* **32,** L03809, doi:10.1029/2004GL021765

Mitas, C. M. and A. Clement, 2006, Recent behavior of the Hadley cell and tropical thermodynamics in climate models and reanalysis, *Goephys. Res. Lett.,* **33**, L01810, doi:10.1029/2005GL024406

Phillips, N. A., 1954, Energy transformations and meridional circulations associated with simple baroclinic waves in a two-level, quasi-geostrophic model, *Tellus VI*, **3,** 273-286

Reichler, T., M. Dameris, and R. Sausen, 2003, Determining the tropopause height from gridded data, *Geophys. Res. Lett.*, **30**(20), 2042, doi:10.1029/2003GLGL018240

Seager, R., N. Harnik, Y. Kushnir, W. Robinson, and J. Miller, 2003, Mechanisms of hemispherically symmetric climate variability. *J. Clim.*, **16**, 2960-2978

Schneider, E. K., 1977, Axially symmetric steady-state models of the basic state for instability and climate studies. Part II. Nonlinear calculations. *J. Atmos. Sci*., **34**, 280-296

Vecchi, G. A. and B. J. Soden, 2006, Global warming and the weakening of the tropical circulation, *J. Clim*. (submitted)

Vecchi, G. A., B. J. Soden, A. T. Wittenberg, I. M. Held, A. Leetmaa, M. J. Harrison, 2005, Weakening of tropical Pacific atmospheric circulation due to anthropogenic forcing, *Nature*, **441**(7089), 73-76.

Williams, G. P. and K. Bryan, 2006, Ice age winds: an aquaplanet model, *J. Clim.*, **19,** 1706-1715

Walker, C. C. and T. Schneider, 2006, Eddy-influences on Hadley circulations: Simulations with a idealized GCM. *J Atmos. Sci.*, in press

World Meteorological Organization (WMO), Meteorology A Three-Dimensional Science: Second Session of the Commission for Aerology, *WMO Bulletin IV (4)*, WMO, Geneva, 134-138, 1957.

Zhang, M. and H. Song, 2006, Evidence of deceleration of atmospheric vertical overturning circulation over the tropical Pacific, *Geophys. Res. Lett.*, **33,** L12701, doi:10.1029/2006GL025942

List of Figures

Figure 1 (a) The multi-model ensemble mean *P-E* in the A2 scenario. Shading indicates the difference between the first and the last 20 years of the 21st century and the black line denotes the 0-isopleths averaged from 2001 to 2020. The right sub-panel shows the zonal mean averaged over 2001-2020 (black) and 2081-2100 (red). Units are mm/day. (b) Number count out of the total 15 models that simulate a moistening (i.e., $\Delta(P-E)>0$) at each grid point.

Figure 2 The breakdown by models and scenarios of the displacement of the northern (warm colors) and southern (cold colors) edges of the subtropical dry zone (y-axis) versus that of the HC (x-axis). The circles, hexagrams, and triangles denote the changes (2081-2100 minus 2001-2020) estimated from the A2, A1B and B1 scenarios, respectively. The open symbols denote the multi-model ensemble mean values.

Figure 3 The fractional change in the intensity of the HC from the beginning (2001-2020) to the end (2081-2100) of the 21st century with respect to the century mean climatology in the models of the A2 scenario. See text for the explanation for the streamfunction-based ($\psi_{500}^{max}-\psi_{500}^{min}$) and omega-based intensity of Hadley circulation ($\int\left(\int\omega_{500}dx\right)^{+}dy$). Each plotted value has been normalized by the change in the global mean temperature within the corresponding model. The unit is %/K.

Figure 4 The relationship of the tropical (20°S-20°N) tropopause height (TTH, left panels); the extra-tropical (35°S-55°S and 35°N-55°N) tropopause height (ETH, right panels) with the extent of the HC for 14 models from the A2 scenario. Positive tropopause height value represents rise of tropopause. Upper panels show the differences between (2081-2020) and (2001-2020), normalized by the corresponding change in the global mean temperature. The red dots denote the multi-model ensemble mean values. Lower panels show the correlation coefficients between the full (blue bars) and detrended (sandy bars) time series of the HC extent and TTH (b) and ETH (d). The dotted lines indicate the P=0.01 confidence level on the correlation based on Student's t-test.

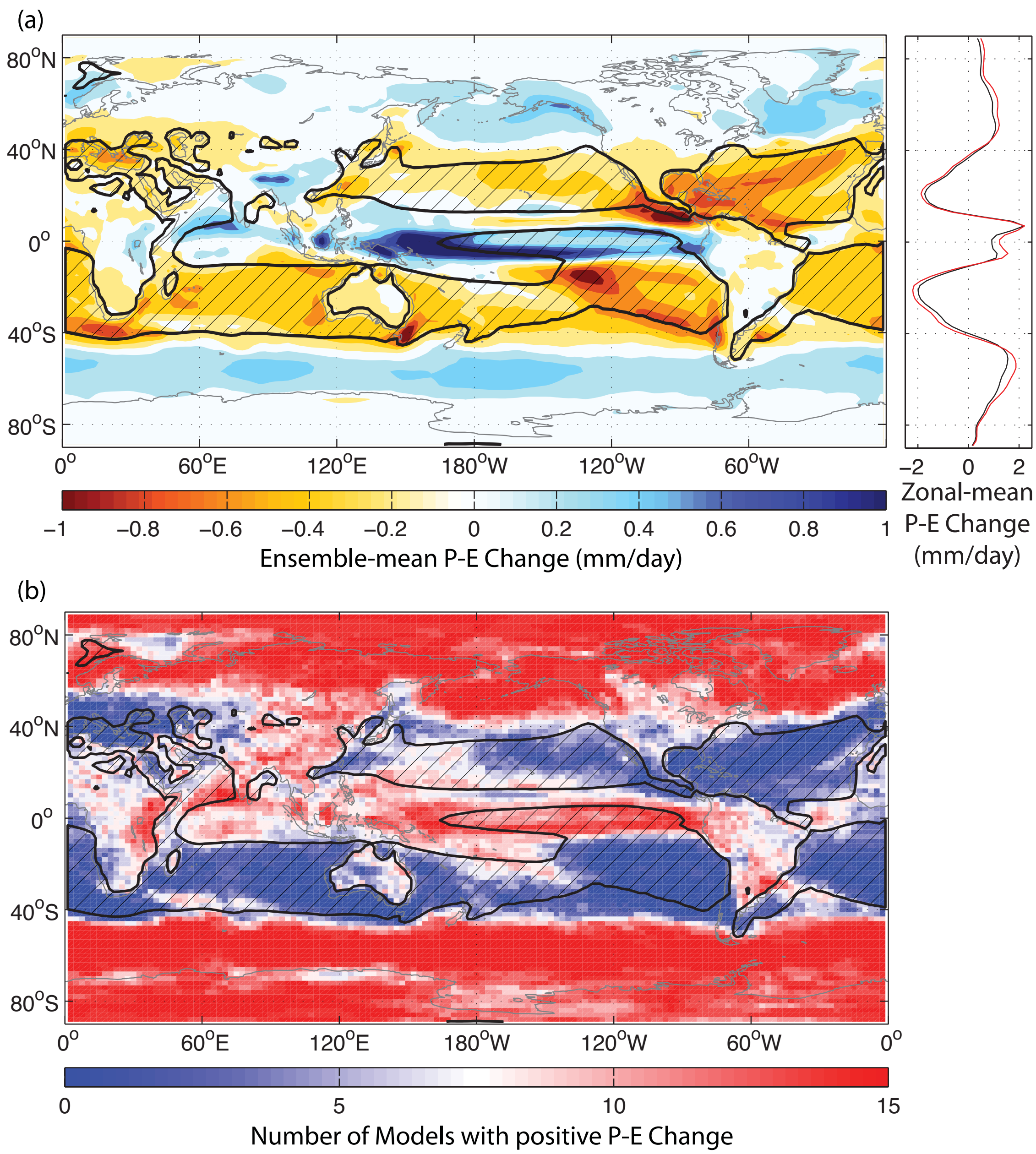

Figure 1 (a) The multi-model ensemble mean *P-E* in the A2 scenario. Shading indicates the difference between the first and the last 20 years of the 21st century and the black line denotes the 0-isopleths averaged from 2001 to 2020. The right sub-panel shows the zonal mean averaged over 2001-2020 (black) and 2081-2100 (red). Units are mm/day. (b) Number count out of the total 15 models that simulate a moistening (i.e., $\Delta(P-E)>0$) at each grid point.

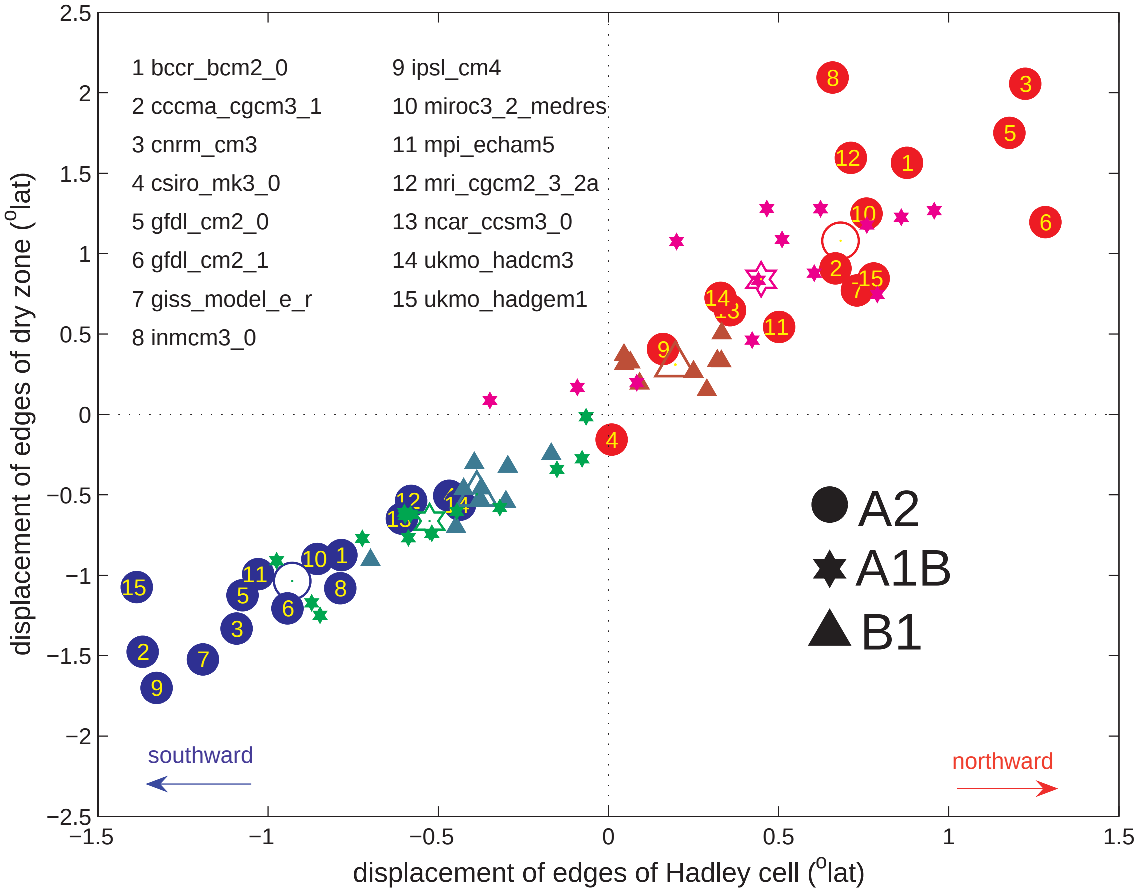

Figure 2 The breakdown by models and scenarios of the displacement of the northern (warm colors) and southern (cold colors) edges of the subtropical dry zone (y-axis) versus that of the HC (x-axis). The circles, hexagrams, and triangles denote the changes (2081-2100 minus 2001-2020) estimated from the A2, A1B and B1 scenarios, respectively. The open symbols denote the multi-model ensemble mean values.

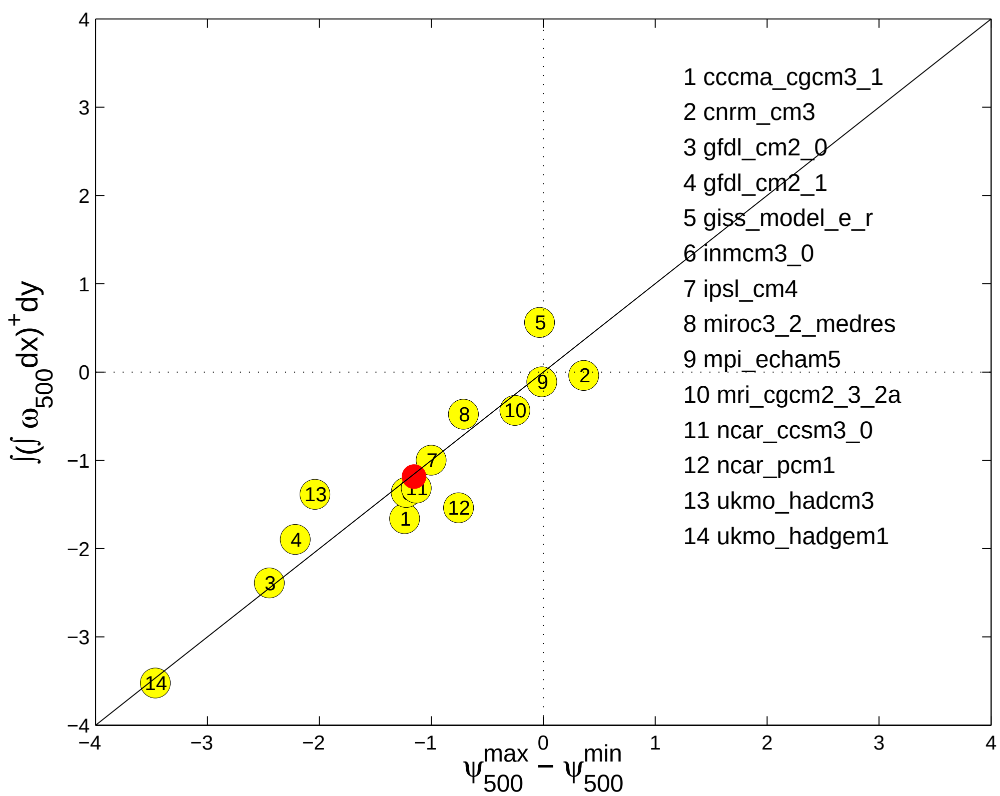

Figure 3 The fractional change in the intensity of the HC from the beginning (2001-2020) to the end (2081-2100) of the 21st century with respect to the century mean climatology in the models of the A2 scenario. See text for the explanation for the streamfunction-based ($\psi_{500}^{max} - \psi_{500}^{min}$) and omega-based intensity of Hadley circulation

($\int\left(\int \omega_{500}dx\right)^{+}dy$). Each plotted value has been normalized by the change in the global mean temperature within the corresponding model. The unit is %/K.

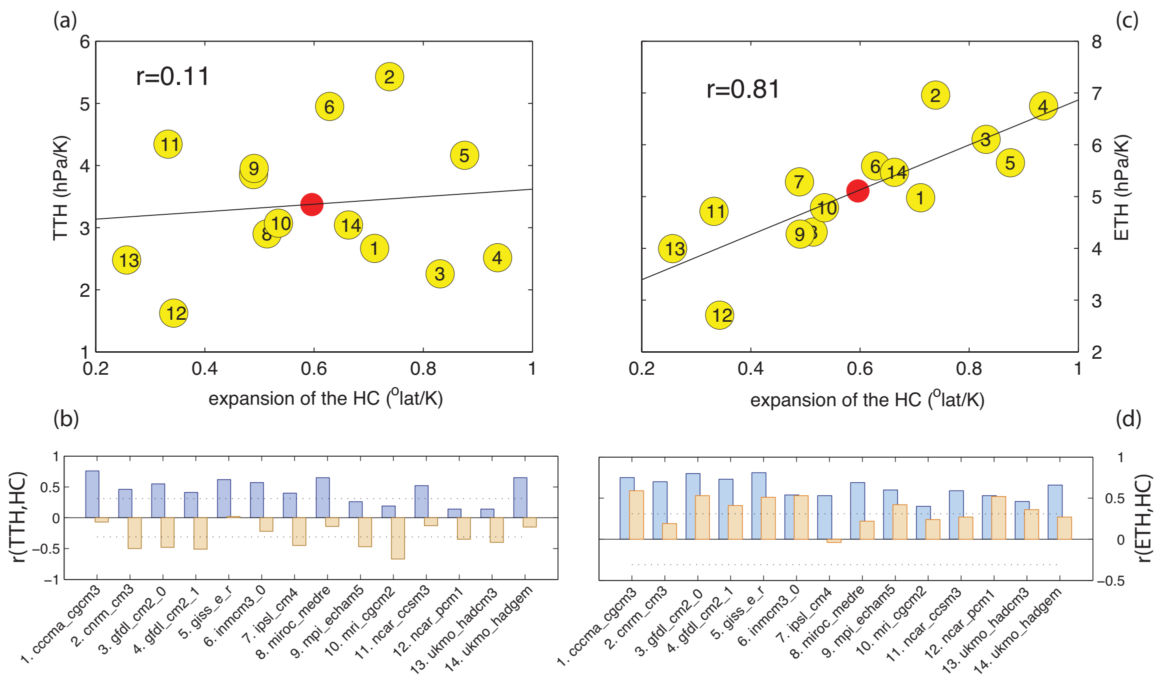

Figure 4 The relationship of the tropical (20°S-20°N) tropopause height (TTH, left panels); the extra-tropical (35°S-55°S and 35°N-55°N) tropopause height (ETH, right panels) with the extent of the HC for 14 models from the A2 scenario. Positive tropopause height value represents rise of tropopause. Upper panels show the differences between (2081-2020) and (2001-2020), normalized by the corresponding change in the global mean temperature. The red dots denote the multi-model ensemble mean values. Lower panels show the correlation coefficients between the full (blue bars) and detrended

(sandy bars) time series of the HC extent and TTH (b) and ETH (d). The dotted lines indicate the P=0.01 confidence level on the correlation based on Student’s t-test.

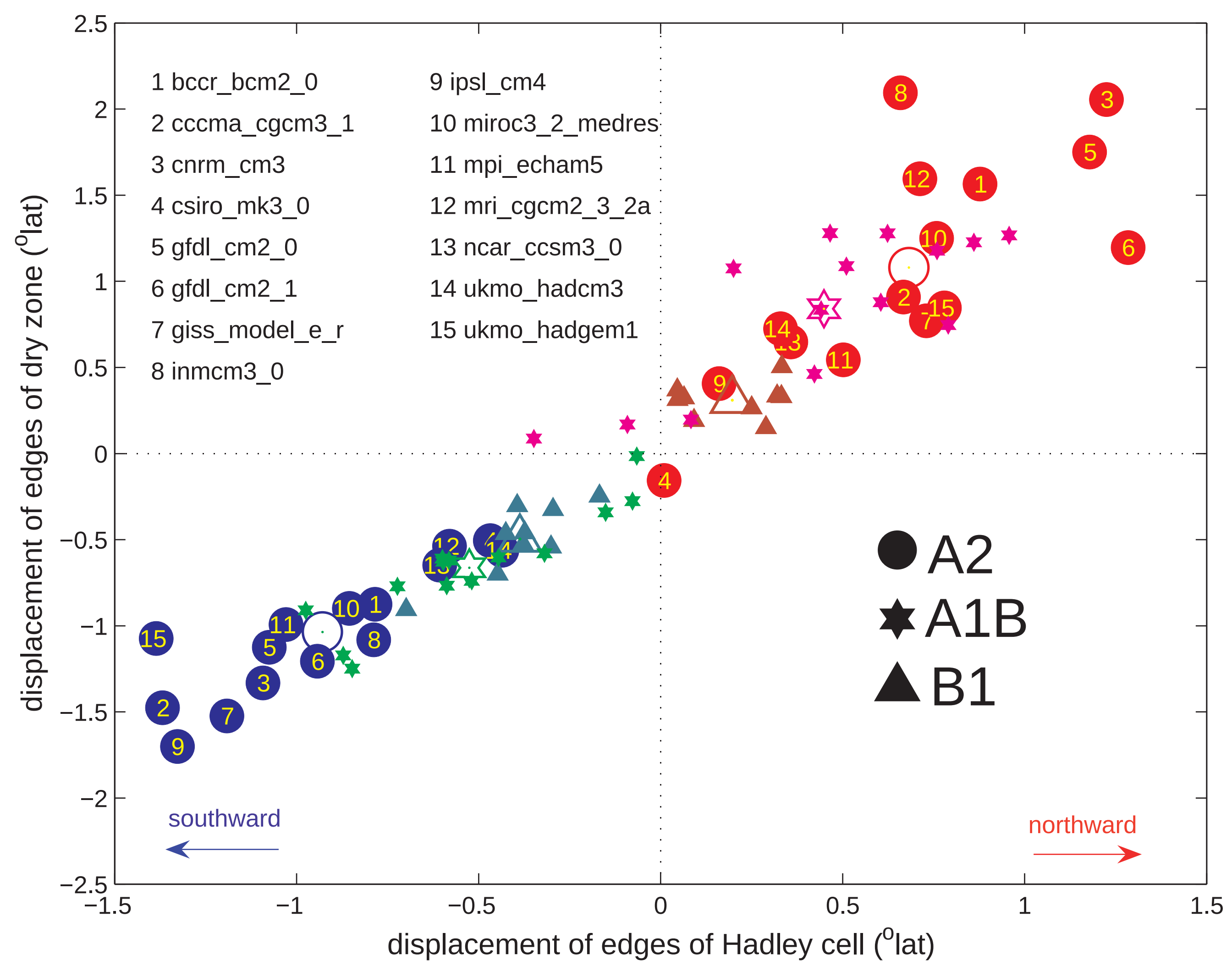

1 bccr_bcm2_0
2 cccma_cgcm3_1
3 cnrm_cm3
4 csiro_mk3_0
5 gfdl_cm2_0
6 gfdl_cm2_1
7 giss_model_e_r
8 inmcm3_0
9 ipsl_cm4
10 miroc3_2_medres
11 mpi_echam5
12 mri_cgcm2_3_2a
13 ncar_ccsm3_0
14 ukmo_hadcm3
15 ukmo_hadgem1
A2
A1B
B1
southward
northward
displacement of edges of dry zone (°lat)
displacement of edges of Hadley cell (°lat)

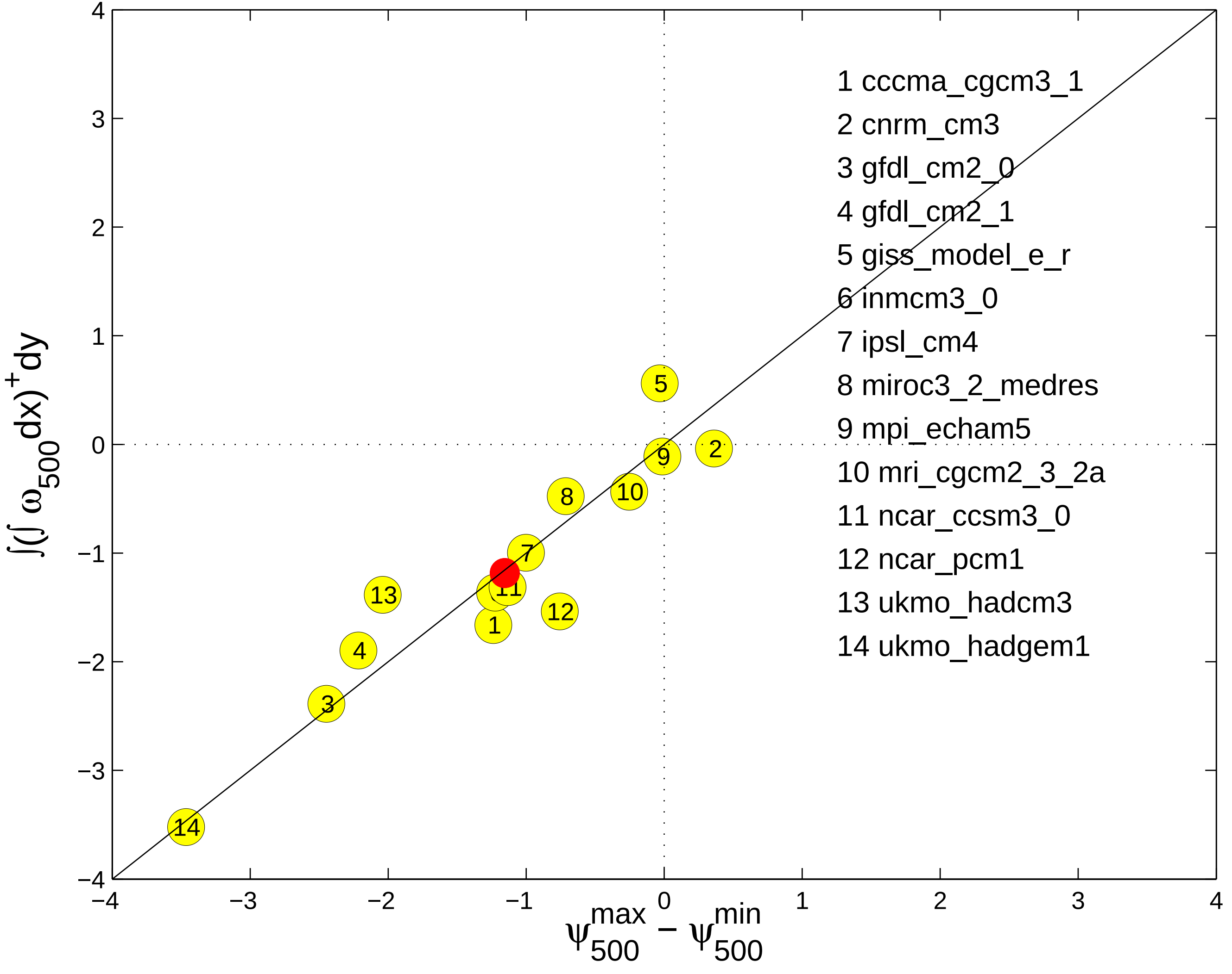

1 cccma_cgcm3_1
2 cnrm_cm3
3 gfdl_cm2_0
4 gfdl_cm2_1
5 giss_model_e_r
6 inmcm3_0
7 ipsl_cm4
8 miroc3_2_medres
9 mpi_echam5
10 mri_cgcm2_3_2a
11 ncar_ccsm3_0
12 ncar_pcm1
13 ukmo_hadcm3
14 ukmo_hadgem1
$\int(\int \omega_{500} dx)^{+} dy$
$\psi_{500}^{max} - \psi_{500}^{min}$

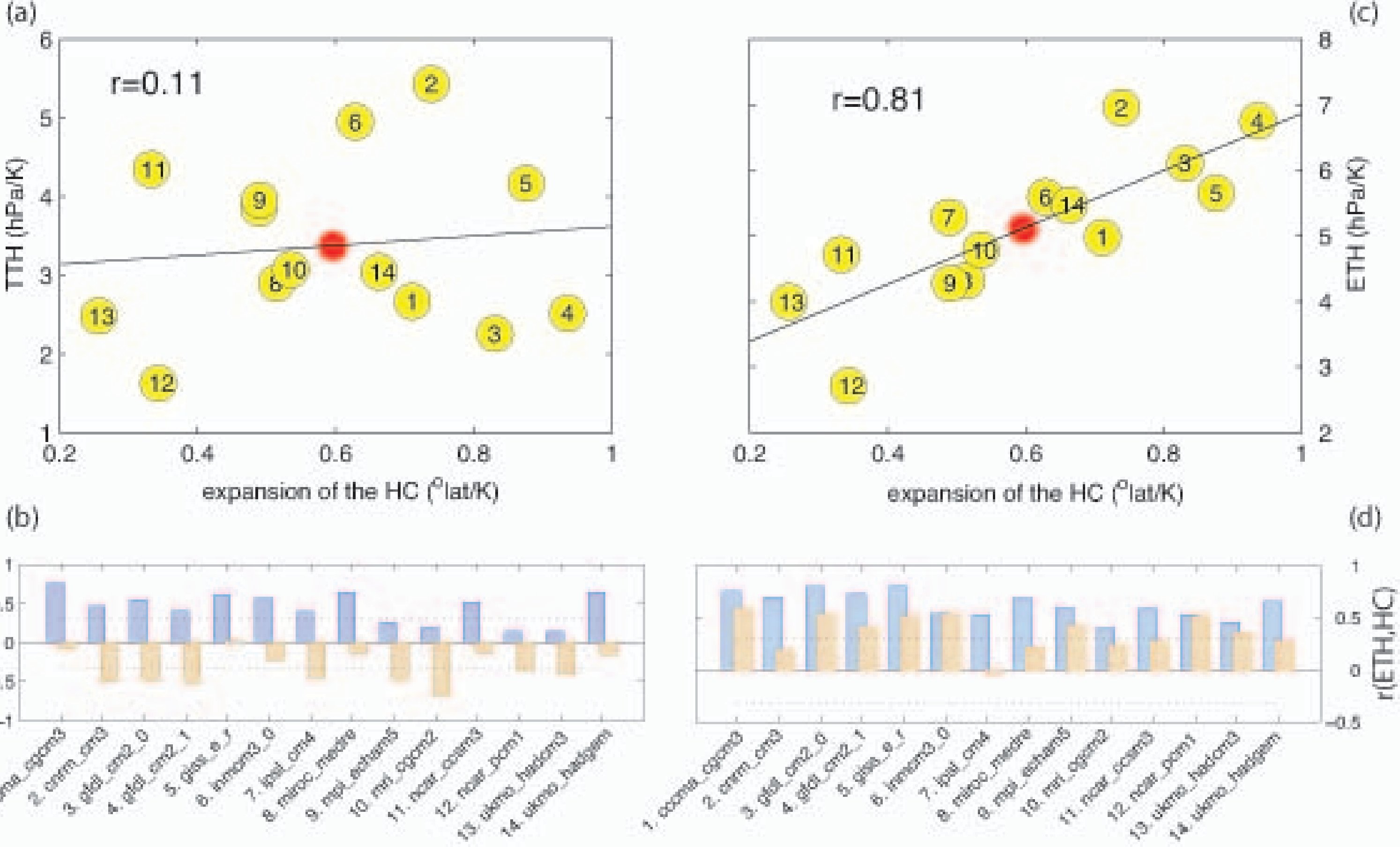

(a)
r=0.11
TTH (hPa/K)
expansion of the HC (°lat/K)
(c)
r=0.81
ETH (hPa/K)
expansion of the HC (°lat/K)
(b)
r(TTH,HC)
(d)
r(ETH,HC)
1. cccma_cgcm3
2. cnrm_cm3
3. gfdl_cm2_0
4. gfdl_cm2_1
5. giss_e_r
6. inmcm3_0
7. ipsl_cm4
8. miroc_medre
9. mpi_echam5
10. mri_cgcm2
11. ncar_ccsm3
12. ncar_pcm1
13. ukmo_hadcm3
14. ukmo_hadgem